Two types of *s*-wave pairing due to magnetic and orbital fluctuations in the two-dimensional 16-band *d-p* model for iron-based superconductors

Yuki Yanagi and Youichi Yamakawa
Department of Physics, Niigata University, Ikarashi, Niigata 950-2181, Japan

Yoshiaki Ōno
Department of Physics, Niigata University, Ikarashi, Niigata 950-2181, Japan
and Center for Transdisciplinary Research, Niigata University, Ikarashi, Niigata 950-2181, Japan

We study superconductivity in the two-dimensional 16-band *d-p* model extracted from a tight-binding fit to the band structure of LaFeAsO, using the random phase approximation. When the intraorbital repulsion U is larger than the interorbital one U', an extended *s*-wave ($s_\pm$-wave) pairing with sign reversal of order parameter is mediated by antiferromagnetic spin fluctuations, while when $U < U'$ another kind of *s*-wave (s_{++}-wave) pairing without sign reversal is mediated by ferro-orbital fluctuations. The s_{++}-wave pairing is enhanced due to the electron-phonon coupling and then can be expanded over the realistic parameter region with $U > U'$.

I. INTRODUCTION

The recently discovered iron-based superconductors[1,2] RFePnO$_{1-x}$F$_x$ (R=rare earth, Pn=As and P) with a transition temperature T_c exceeding 50 K (Refs. [3–7]) have attracted much attention. The F nondoped compound LaFeAsO exhibits the structural transition from tetragonal ($P4/nmm$) to orthorhombic ($Cmma$) phase at a transition temperature T=155 K and stripe-type antiferromagnetic order at T=134 K with a magnetic moment $\sim 0.36\mu_B$ (Ref. [8]) at low temperature. With increasing F doping, the system becomes metallic and the antiferromagnetic order disappears,[2] and then, the superconductivity emerges for $x \sim 0.1$ with $T_c \sim 26$ K. Rare-earth substitution compounds exhibit superconducting transition with higher T_c.[3–7] Specific features of the systems are two-dimensionality of the conducting Fe$_2$As$_2$ plane and the orbital degrees of freedom in Fe^{2+} ($3d^6$).[1,2] The pairing symmetry together with the mechanism of the superconductivity is one of the most significant issues.

The NMR Knight shift measurements revealed that the superconductivity of the systems is the spin-singlet pairing.[9,10] Fully gapped superconducting states have been predicted by various experiments such as the penetration depth,[11] the specific heat,[12] the angle-resolved photoemission spectroscopy (ARPES),[13–15] and the impurity effect on T_c.[10,16] In contrast to the above-mentioned experiments, the NMR relaxation rate shows the power-law behavior $1/T_1 \propto T^3$ below T_c,[17] suggesting the nodal or highly anisotropic gap structure. The other NMR measurements,[18] however, revealed $1/T_1 \propto T^6$ below T_c and there is still controversy.

Theoretically, the first-principles calculations have predicted that the nondoped system is metallic with two or three concentric hole Fermi surfaces around the Γ point [$\mathbf{k}$=(0,0)] and two elliptical electron Fermi surfaces around the M point [$\mathbf{k}$=(π,π)].[19–23] Mazin *et al.*[24] suggested that the spin-singlet extended *s*-wave pairing whose order parameter changes its sign between the hole pockets and the electron pockets ($s_\pm$ wave) is favored due to the antiferromag-

netic spin fluctuations. According to the weak coupling approaches based on multiorbital Hubbard models,[25–34] the $s_\pm$-wave pairing or the d_{xy}-wave pairing is expected to emerge. It is shown that the $s_\pm$-wave pairing is realized also in the strong coupling region by the mean-field study based on the t-J_1-J_2 model[35] and the exact diagonalization study based on the one-dimensional two-band Hubbard model.[36]

Generally speaking, the details of the band structure and the Fermi surface are crucial for determining the pairing symmetry. In the five-band Hubbard model originally introduced by Kuroki *et al.*,[25] the energy bands obtained by reproduce those obtained by the density functional calculation very well. In this model, however, the spatial extensions of the Fe 3*d*-like Wannier orbitals are different from each other[37] and the resulting intraorbital terms of the on-site Coulomb interaction are strongly orbital dependent.[38] In addition, since the model explicitly includes the transfer integrals up to the fifth nearest-neighbor sites,[25] one should take the off-site Coulomb interaction, which is considered to be about 0.5 eV between the nearest-neighbor sites, into account to ensure the consistency of the model.[38] On the other hand, in the effective model which includes both the Fe 3*d* orbitals and the As 4*p* orbitals, so called *d-p* model, the spatial extensions and the differences in those between the orbitals will be considerably reduced.[37] Due to these facts, in the *d-p* model, it is expected that the intraorbital terms of the on-site Coulomb interaction for each orbitals have almost the same values and the off-site Coulomb interaction are negligible. Therefore, theoretical studies based on the *d-p* model, are highly desired.

In the previous papers,[39,40] we have investigated the electronic states of the Fe$_2$As$_2$ plane in iron-based superconductors on the basis of the two-dimensional 16-band *d-p* model which includes the Coulomb interaction on a Fe site: the intraorbital and interorbital direct terms U and U', the Hund's coupling J and the pair-transfer J'. Using the random phase approximation (RPA), we have found that, for a larger value of J, the most favorable pairing symmetry is $s_\pm$ wave, while, for a smaller value of J, it is d_{xy} wave.
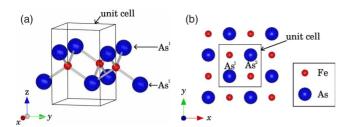
FIG. 1. (Color online) Crystal structure of Fe_2As_2 layer. Small and large balls represent Fe and As atoms, respectively. The solid line represents the unit cell. It is noted that As^1 and As^2 denote the As atoms on the upper side and on the lower side of the Fe_2As_2 layer, respectively.

The present paper is a full paper to our previous papers[39,40] with some numerical improvements.[40] In the present paper, we investigate the superconductivity in the wider parameter space by treating U, U', J, and J' as independent parameters in contrast to the previous study under the condition that $U=U'+2J$ and $J=J'$ based on the two-dimensional 16-band d-p model. Solving the superconducting gap equation with the pairing interaction obtained by using the RPA, we find that two kinds of the s-wave superconducting states appear. As above mentioned, the $s_{\pm}$-wave superconducting state emerges near the incommensurate spin density wave (ISDW) with $\mathbf{q} \sim (\pi, \pi)$ phase. In addition, for $U < U'$, the s-wave superconducting state appears around the ferro-orbital ordered phase. The order parameter for this s-wave state dose not change its sign in $\mathbf{k}$ space. We refer to this s-wave state as the s_{++}-wave state, hereafter.

II. MODEL AND FORMULATION

First of all, we perform the density-functional calculation for LaFeAsO with the generalized gradient approximation of Perdew, Burke, and Ernzerhof[41] by using the WIEN2K package,[42] where the lattice parameters ($a=4.03268$ Å and $c=8.74111$ Å) and the internal coordinates ($z_{La}=0.14134$ and $z_{As}=0.65166$) are experimentally determined.[43] The crystal structure of Fe_2As_2 layer is shown in Fig. 1(a). Since As atoms are tetrahedrally arranged around a Fe atom, there are two distinct Fe and As sites in the crystallographic unit cell [see Figs. 1(a) and 1(b)]. Considering these facts, we then derive the two-dimensional 16-band d-p model,[39] where 3d orbitals ($d_{3z^2-r^2}$, $d_{x^2-y^2}$, d_{xy}, d_{yz}, and d_{zx}) of two Fe atoms ($Fe^1=A$ and $Fe^2=B$) and 4p orbitals (p_x, p_y, and p_z) of two As atoms are explicitly included. We note that x and y axes are directed along second nearest Fe-Fe bonds [see Fig. 1(b)].

The total Hamiltonian of the d-p model is given by

$$H = H_0 + H_{\text{int}}, \tag{1}$$

where H_0 and H_{int} are the noninteracting and interacting parts of the Hamiltonian, respectively. The noninteracting part of the d-p model is given by the following tight-binding Hamiltonian:

$$H_0 = \sum_{i,\ell,\sigma} \varepsilon_\ell^d d_{i\ell\sigma}^\dagger d_{i\ell\sigma} + \sum_{i,m,\sigma} \varepsilon_m^p p_{im\sigma}^\dagger p_{im\sigma}$$
$$+ \sum_{i,j,\ell,\ell',\sigma} t_{i,j,\ell,\ell'}^{dd} d_{i\ell\sigma}^\dagger d_{j\ell'\sigma} + \sum_{i,j,m,m',\sigma} t_{i,j,m,m'}^{pp} p_{im\sigma}^\dagger p_{jm'\sigma}$$
$$+ \sum_{i,j,\ell,m,\sigma} t_{i,j,\ell,m}^{dp} d_{i\ell\sigma}^\dagger p_{jm\sigma} + \text{H.c.}, \tag{2}$$

where $d_{i\ell\sigma}$ is the annihilation operator for Fe 3d electrons with spin σ in the orbital ℓ at the site i and $p_{im\sigma}$ is the annihilation operator for As 4p electrons with spin σ in the orbital m at the site i. In Eq. (2), the transfer integrals $t_{i,j,\ell,\ell'}^{dd}$, $t_{i,j,m,m'}^{pp}$, $t_{i,j,\ell,m}^{dp}$, and the atomic energies ε_ℓ^d, ε_m^p are determined so as to fit both the energy and the weights of orbitals for each band obtained from the tight-binding approximation to those from the density-functional calculation.[44] Similar models have been used by the other authors[34,45,46] but the model parameters are different from ours. The doping concentration x corresponds to the number of electrons per unit cell $n=24+2x$ in the present model.

Now we consider the effect of the Coulomb interaction on Fe site. The interacting part of the Hamiltonian is given as follows:

$$H_{\text{int}} = \frac{1}{2} U \sum_i \sum_\ell \sum_{\sigma \neq \bar{\sigma}} d_{i\ell\sigma}^\dagger d_{i\ell\bar{\sigma}}^\dagger d_{i\ell\bar{\sigma}} d_{i\ell\sigma}$$
$$+ \frac{1}{2} U' \sum_i \sum_{\ell \neq \bar{\ell}} \sum_{\sigma,\sigma'} d_{i\ell\sigma}^\dagger d_{i\bar{\ell}\sigma'}^\dagger d_{i\bar{\ell}\sigma'} d_{i\ell\sigma}$$
$$+ \frac{1}{2} J \sum_i \sum_{\ell \neq \bar{\ell}} \sum_{\sigma,\sigma'} d_{i\ell\sigma}^\dagger d_{i\bar{\ell}\sigma'}^\dagger d_{i\ell\sigma'} d_{i\bar{\ell}\sigma}$$
$$+ \frac{1}{2} J' \sum_i \sum_{\ell \neq \bar{\ell}} \sum_{\sigma \neq \bar{\sigma}} d_{i\ell\sigma}^\dagger d_{i\ell\bar{\sigma}}^\dagger d_{i\bar{\ell}\bar{\sigma}} d_{i\bar{\ell}\sigma}, \tag{3}$$

where U and U' are the intraorbital and interorbital direct terms, respectively, and J and J' are the Hund's coupling and the pair transfer, respectively. For the isolated atoms, the relations between Coulomb matrix elements $U=U'+2J$ and $J=J'$ are derived due to the rotational invariance of the Coulomb interaction and the reality of the wave functions, respectively.[47] For the atoms in the crystal, however, the relation is not satisfied generally due to the crystallographic effects and the many-body effects due to the Coulomb interaction and the electron-phonon coupling which will be discussed later. Therefore, we treat U, U', J, and J' as independent parameters in the present paper.

Within the RPA,[48–50] the spin susceptibility $\hat{\chi}^s(\mathbf{q})$ and the charge-orbital susceptibility $\hat{\chi}^c(\mathbf{q})$ are given in the 50×50 matrix representation as follows:[39]

$$\hat{\chi}^s(\mathbf{q}) = [\hat{1} - \hat{\chi}^{(0)}(\mathbf{q})\hat{S}]^{-1}\hat{\chi}^{(0)}(\mathbf{q}), \tag{4}$$

$$\hat{\chi}^c(\mathbf{q}) = [\hat{1} + \hat{\chi}^{(0)}(\mathbf{q})\hat{C}]^{-1}\hat{\chi}^{(0)}(\mathbf{q}) \tag{5}$$

with the noninteracting susceptibility

$$\chi^{(0)\alpha,\beta}_{\ell_1\ell_2,\ell_3\ell_4}(\mathbf{q}) = -\frac{1}{N}\sum_{\mathbf{k}}\sum_{\mu,\nu}\frac{f(\varepsilon_{\mathbf{k+q},\mu})-f(\varepsilon_{\mathbf{k},\nu})}{\varepsilon_{\mathbf{k+q},\mu}-\varepsilon_{\mathbf{k},\nu}}$$
$$\times u^{\alpha}_{\ell_1,\nu}(\mathbf{k})^* u^{\alpha}_{\ell_2,\mu}(\mathbf{k+q}) u^{\beta}_{\ell_3,\nu}(\mathbf{k}) u^{\beta}_{\ell_4,\mu}(\mathbf{k+q})^*,$$

(6)

where μ, $\nu(=1-16)$ are band indexes, α, β ($=A,B$) represent two Fe sites, ℓ represents Fe 3d orbitals, $u^{\alpha}_{\ell,\mu}(\mathbf{k})$ is the eigenvector which diagonalizes H_0 Eq. (2), $\varepsilon_{\mathbf{k},\mu}$ is the corresponding eigenenergy of band μ with wave vector $\mathbf{k}$ and $f(\varepsilon)$ is the Fermi distribution function. In Eqs. (4) and (5), the interaction matrix $\hat{S}$ ($\hat{C}$) is given by

$$\hat{S}(\hat{C}) = \begin{cases} U(U) & (\alpha=\beta,\ell_1=\ell_2=\ell_3=\ell_4) \\ U'(-U'+2J) & (\alpha=\beta,\ell_1=\ell_3\neq\ell_2=\ell_4) \\ J(2U'-J) & (\alpha=\beta,\ell_1=\ell_2\neq\ell_3=\ell_4) \\ J'(J') & (\alpha=\beta,\ell_1=\ell_4\neq\ell_2=\ell_3) \\ 0 & (\text{otherwise}). \end{cases}$$

(7)

In the weak coupling regime, the superconducting gap equation is given by[39]

$$\lambda\Delta^{\alpha\beta}_{\ell\ell'}(\mathbf{k}) = \frac{1}{N}\sum_{\mathbf{k'}}\sum_{\ell_1\ell_2\ell_3\ell_4}\sum_{\alpha',\beta'}\sum_{\mu,\nu}\times\frac{f(\varepsilon_{-\mathbf{k'},\mu})+f(\varepsilon_{\mathbf{k'},\nu})-1}{\varepsilon_{-\mathbf{k'},\mu}+\varepsilon_{\mathbf{k'},\nu}}$$
$$\times V^{\alpha,\beta}_{\ell\ell_1,\ell_2\ell'}(\mathbf{k}-\mathbf{k'})\Delta^{\alpha'\beta'}_{\ell_3\ell_4}(\mathbf{k'})$$
$$\times u^{\alpha'}_{\ell_3,\mu}(-\mathbf{k'})u^{\alpha}_{\ell_1,\mu}(-\mathbf{k'})^* u^{\beta'}_{\ell_4,\nu}(\mathbf{k'})u^{\beta}_{\ell_2,\nu}(\mathbf{k'})^*,$$

(8)

where $\Delta^{\alpha\beta}_{\ell\ell'}(\mathbf{k})$ is the gap function and $V^{\alpha,\beta}_{\ell_1\ell_2,\ell_3\ell_4}(\mathbf{q})$ is the effective pairing interaction.[51] Within the RPA,[48–50] $V^{\alpha,\beta}_{\ell_1\ell_2,\ell_3\ell_4}(\mathbf{q})$ is given in the 50×50 matrix

$$\hat{V}(\mathbf{q}) = \eta\left[\hat{S}\hat{\chi}^s(\mathbf{q})\hat{S}+\frac{1}{2}\hat{S}\right]-\frac{1}{2}\left[\hat{C}\hat{\chi}^c(\mathbf{q})\hat{C}-\frac{1}{2}\hat{C}\right],$$

(9)

where $\eta=\frac{3}{2}$ for the spin-singlet state and $\eta=-\frac{1}{2}$ for the spin-triplet state. The gap in Eq. (8) is solved to obtain the gap function $\Delta^{\alpha\beta}_{\ell\ell'}(\mathbf{k})$ with the eigenvalue λ. At $T=T_c$, the largest eigenvalue λ becomes unity. In the present paper, we only focus on the case with $x=0.1$, where the superconductivity is observed in the compounds.[2] For simplicity, we set $x=0.1$ and $T=0.02$ eV in the present study. We use 32×32 **K** points in the numerical calculations for Eqs. (4)–(9) and also use the fast Fourier transformation to solve the gap equation, Eq. (8). Here and hereafter, we measure the energy in units of eV.

III. CALCULATED RESULTS

A. Band structure

We show the band structure obtained from the d-p tight-binding Hamiltonian Eq. (2), where the tight-binding parameters are listed in Table I,[44] together with that obtained from the density-functional calculation in the Fig. 2(a). The result of our density-functional calculation is similar to that previously reported by the other authors.[19–23,25] It is found that the former reproduces the latter very well. We note that the

TABLE I. Tight-binding parameters (in units of eV) for the d-p Hamiltonian (2). It is noted that we define the d-p hopping and the in-plane p-p hopping parameters along x axis.

On-site energy		
$d_{3z^2-r^2}$	−0.687	
$d_{x^2-y^2}$	−0.610	
d_{xy}	−0.921	
d_{yz}	−0.820	
p_x	−1.789	
p_z	−2.173	

d-d hopping	Nearest	Next nearest
$d_{3z^2-r^2}$-$d_{3z^2-r^2}$	−0.008	−0.024
$d_{x^2-y^2}$-$d_{x^2-y^2}$	0.143	−0.023
d_{xy}-d_{xy}	0.328	0.073
d_{yz}-d_{yz}	0.109	−0.012
d_{zx}-d_{zx}	0.109	0.012
$d_{3z^2-r^2}$-d_{xy}	0.078	
$d_{3z^2-r^2}$-$d_{x^2-y^2}$		−0.184
d_{yz}-d_{zx}	0.184	

p-p hopping	As^1-As^1	As^1-As^2
p_x-p_x	0.650	0.311
p_y-p_y	0.027	0.311
p_z-p_z	0.048	0.389
p_x-p_y		0.111
p_x-p_z		0.297

d-p hopping	Nearest
$d_{3z^2-r^2}$-p_x	0.646
$d_{3z^2-r^2}$-p_z	−0.291
$d_{x^2-y^2}$-p_x	0.276
$d_{x^2-y^2}$-p_z	0.563
d_{xy}-p_y	0.694
d_{yz}-p_y	0.319
d_{zx}-p_x	0.783
d_{zx}-p_z	0.164

weights of orbitals also agree very well with each other (not shown). Due to the weak crystalline electric field from the As^{3-} ions tetrahedrally arranged around a Fe atom and the strong hybridization between the Fe 3d orbitals, the resulting energy bands have very complicated structure.

The Fermi surface for the d-p tight-binding Hamiltonian is shown in Fig. 2(b), where we can see nearly circular hole pockets around the Γ point and elliptical electron pockets around the M point. These results are consistent with the previous first-principles calculations.[19–23]

The density of states (DOS) obtained by the d-p tight-binding Hamiltonian Eq. (2) is shown in Fig. 2(c). It is found that the dominant contribution near the Fermi level comes from Fe 3d orbitals and the contribution of As 4p orbitals is
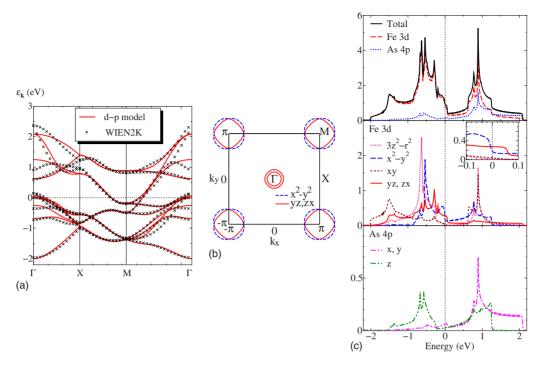
FIG. 2. (Color online) (a) The band structure obtained from the d-p model, Eq. (2), (solid line) and that obtained from the density-functional calculation (cross) for $x=0.1$. (b) Fermi surface obtained from the d-p model for $x=0.1$. The solid and dashed lines show the Fermi surfaces which have mainly d_{yz}, d_{zx} and $d_{x^2-y^2}$ orbital character, respectively. (c) The DOS obtained from the d-p model for $x=0.1$. Upper panel: total DOS, middle panel: partial DOS of the Fe $3d$ orbitals, and lower panel: partial DOS of the As $4p$ orbitals. The inset of the middle panel shows the DOS near the Fermi level. We note that the Fermi level set to 0 on the energy axis.

small but is not negligible. We show the partial DOS of Fe $3d$ orbitals and that of As $4p$ orbitals in the middle panel and the lower panel of Fig. 2(c), respectively. The d_{yz}, d_{zx}, and $d_{x^2-y^2}$ states comprise the large part of the DOS near the Fermi level, while, the $d_{3z^2-r^2}, d_{xy}$ states occupy the small one and are comparable with the p_x, p_y, and p_z states. The d_{yz} and d_{zx} states at the Fermi level are larger than the $d_{x^2-y^2}$ ones and this corresponds to the fact that the electron pockets have d_{yz}, d_{zx}, and $d_{x^2-y^2}$ orbital characters, while, the hole pockets have only d_{yz} and d_{zx} orbital characters. However, the $d_{x^2-y^2}$ states have large values just below the Fermi level as shown in the inset of the middle panel of Fig. 2(c). This is due to the hole band near the Γ point just below the Fermi level. Therefore, it is anticipated that the d_{yz}, d_{zx}, and $d_{x^2-y^2}$ orbitals play significant roles to determine the magnetic, orbital, and superconducting properties.

B. RPA results for $U>U'$

In this section, we concentrate our attention on the case with $U>U'$. We set the typical parameters as $U=1.71$, $U'=1.4$, and $J=J'=0.1$, where the condition for the superconducting transition $\lambda=1$ is satisfied as mentioned below [see Fig. 3(d)]. The several components of the spin susceptibility $\hat{\chi}^s(\mathbf{q})$ given in Eq. (4) are plotted in Fig. 3(a). The spin susceptibility is enhanced due to the effect of the Coulomb interaction. It is found that the most dominant component is the $d_{x^2-y^2}$ diagonal component and the incommensurate peaks around the M point are observed as reflecting the nesting between the hole pockets and the electron pockets. As mentioned before, the hole band which has mainly $d_{x^2-y^2}$ orbital character exists just below (~ 0.01 eV) the Fermi level and contributes to the large value of the DOS [see Fig. 2(c)]. Therefore, the $d_{x^2-y^2}$ diagonal component of
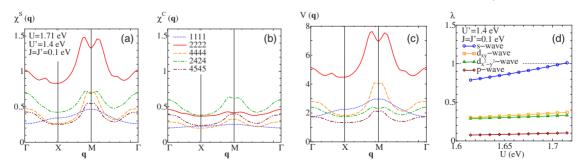

FIG. 3. (Color online) (a) Several components of the spin susceptibility $\hat{\chi}^s(\mathbf{q})$, (b) the charge-orbital susceptibility $\hat{\chi}^c(\mathbf{q})$, and (c) the effective pairing interaction $\hat{V}(\mathbf{q})$ in $\mathbf{q}$ space for $U=1.71$, $U'=1.4$, and $J=J'=0.1$ eV. It is noted that we number the orbitals as follows: (1) $d_{3z^2-r^2}$, (2) $d_{x^2-y^2}$, (3) d_{xy}, (4) d_{yz}, and (5) d_{zx}. (d) U dependence of the eigenvalues of the gap equation for several symmetries.
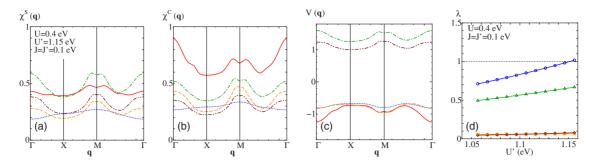
FIG. 4. (Color online) (a) Several components of the spin susceptibility $\hat{\chi}^s(\mathbf{q})$, (b) the charge-orbital susceptibility $\hat{\chi}^c(\mathbf{q})$, and (c) the effective pairing interaction $\hat{V}(\mathbf{q})$ in $\mathbf{q}$ space for $U=0.4$, $U'=1.15$, and $J=J'=0.1$ eV. It is noted that (d) U' dependence of the eigenvalues of the gap equation for several symmetries. It is noted that the legends are the same as Fig. 3.

$\hat{\chi}^s(\mathbf{q})$ becomes most dominant at finite temperature $T=0.02$ eV (>0.01 eV). The result is consistent with the RPA results based on the five-band Hubbard model.[25]

The several components of the charge-orbital susceptibility $\hat{\chi}^c(\mathbf{q})$ given in Eq. (5) are plotted in Fig. 3(b). In contrast to the case with the spin susceptibility, the off-diagonal component of $d_{x^2-y^2}-d_{yz}$ which corresponds to the transverse orbital susceptibility becomes most dominant and shows peaks around the M point together with those at the Γ point. It is noted that for $U>U'$ the spin fluctuations dominate over the charge-orbital fluctuations as shown in Figs. 3(a) and 3(b).

The several components of the effective pairing interaction $\hat{V}(\mathbf{q})$ for the spin-singlet state given in Eq. (9) are plotted in Fig. 3(c). Since the largest eigenvalue λ is always spin-singlet state in the present study, we show the effective pairing interaction only for the spin-singlet state. Since in the case for $U=1.71$, $U'=1.4$, and $J=J'=0.1$, the spin fluctuations dominate over the orbital fluctuations as mentioned above, the structures of $\hat{V}(\mathbf{q})$ are similar to those of the spin susceptibility.

Substituting $\hat{V}(\mathbf{q})$ into the gap equation, Eq. (8), we obtain the gap function $\hat{\Delta}(\mathbf{k})$ with the eigenvalue λ. In Fig. 3(d), the eigenvalues λ for various pairing symmetries are plotted as functions of U for fixed values of U', J, and J'. With increasing U, λ monotonically increases and finally becomes unity at a critical value U_c above which the superconducting state is realized. For $U'=1.4$ and $J=J'=0.1$ the largest eigenvalue λ is for the *s*-wave symmetry and $U_c=1.71$. The second largest eigenvalue is for d_{xy}-wave symmetry and the eigenvalue for the d_{xy}-wave symmetry increases as J increases for $U>U'$.

C. RPA results for $U<U'$

In this section, we concentrate our attention on the case with $U<U'$. We set the typical parameters as $U=0.4$, $U'=1.15$, and $J=J'=0.1$, where the condition for the superconducting transition $\lambda=1$ is satisfied as mentioned below [see Fig. 4(d)].

The several components of the spin susceptibility $\hat{\chi}^s(\mathbf{q})$ given in Eq. (4) are plotted in Fig. 4(a). In contrast to the case with $U>U'$ [see Fig. 3(a)], the off-diagonal element $d_{x^2-y^2}-d_{yz}$ is most dominant owing to the interorbital direct term $U'>U$.

The several components of the charge-orbital susceptibility $\hat{\chi}^c(\mathbf{q})$ given in Eq. (5) are plotted in Fig. 4(b). In contrast to the case with the spin susceptibility, the diagonal component of $d_{x^2-y^2}$ becomes most dominant and shows peaks around the Γ point. It is noted that for $U<U'$ the charge-orbital fluctuations, which corresponds to the fluctuations near the ferro-orbital ordered state realized in the large U' regime as mentioned later (see Fig. 8), dominate over the spin fluctuations as shown in Figs. 4(a) and 4(b).

The several components of the effective pairing interaction $\hat{V}(\mathbf{q})$ for the spin-singlet state given in Eq. (9) are plotted in Fig. 4(c). Since for $U=0.4$, $U'=1.15$, and $J=J'=0.1$, the charge-orbital fluctuations are larger than the spin fluctuations, the diagonal components of $\hat{V}(\mathbf{q})$ are always negative in $\mathbf{q}$ space.

Substituting $\hat{V}(\mathbf{q})$ into the gap equation, Eq. (8), we obtain the gap function $\hat{\Delta}(\mathbf{k})$ with the eigenvalue λ. In Fig. 4(d), the eigenvalues λ for various pairing symmetries are plotted as functions of U' for fixed values of U, J, and J'. With increasing U', λ monotonically increases and finally becomes unity at a critical value $U'_c=1.15$ above which the superconducting state is realized. Similar to the case of $U>U'$, the largest eigenvalue λ is for the *s*-wave symmetry but the superconducting gap structure is significantly different from that for $U>U'$ as shown below.

D. Gap functions

First, we discuss the gap functions in the case with $U>U'$. Figure 5 shows the diagonal components of the gap function $\hat{\Delta}(\mathbf{k})$ for $U=1.71$, $U'=1.4$, and $J=J'=0.1$. Figures 5(a)–5(d) show the gap functions in the orbital representation and Figs. 5(e)–5(h) show those in the band representation. We note that the energy bands are numbered as descending energy. It is found that the gap function has the *s*-wave symmetry and the most dominant component is the $d_{x^2-y^2}$ diagonal component. We find that the gap functions in the band representation have different signs between the electron pockets and the hole pockets without any nodes on the Fermi surfaces ($s_\pm$-wave symmetry).[24–34] It is noted that the diagonal components of the gap function in the orbital representation, except for the d_{xy} component, also change those signs in $\mathbf{k}$ space. The absolute values of the gap functions on the
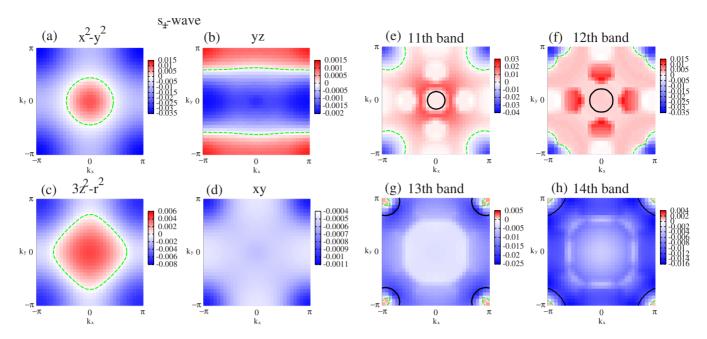
FIG. 5. (Color online) [(a)–(d)] The diagonal components of the gap function $\hat{\Delta}(\mathbf{k})$ in the orbital representation and [(e)–(h)] those in the band representation for $U=1.71$, $U'=1.4$, and $J=J'=0.1$ eV. The solid and dashed lines represent the Fermi surfaces and the nodes of the gap function, respectively.

Fermi surfaces are almost isotropic but largely depend on the energy bands; those on the electron pockets of the 13th and 14th bands are twice or more larger than those on the hole pockets of the 11th and 12th bands. This is because the $d_{x^2-y^2}$ component, which has dominant contribution in $\hat{\chi}^s(\mathbf{q})$ as shown in Fig. 3(a), for the 13th and 14th bands is larger than that for the 11th and 12th bands. We note that the tenth band (hole band) with the largest $d_{x^2-y^2}$ component has the largest absolute value of the gap function although the Fermi

level is just above the tenth band and does not cross it for $x=0.1$.

Next, we discuss the gap functions in the case with $U<U'$. Figure 6 shows the diagonal components of the gap function $\hat{\Delta}(\mathbf{k})$ for $U=0.4$, $U'=1.15$, and $J=J'=0.1$. Figures 6(a)–6(d) shows the gap functions in the orbital representation and Figs. 6(e)–6(h) show those in the band representation. The diagonal components of the gap function in the orbital representation have no sign change in the $\mathbf{k}$ space due
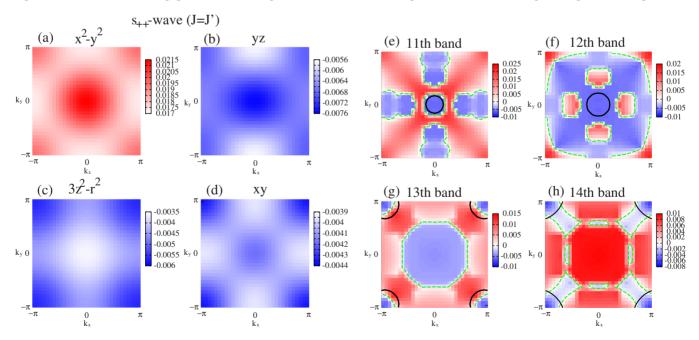

FIG. 6. (Color online) [(a)–(d)] The diagonal components of the gap function $\hat{\Delta}(\mathbf{k})$ in the orbital representation and [(e)–(h)] those in the band representation for $U=0.4$, $U'=1.15$, and $J=J'=0.1$ eV. The solid and dashed lines represent the Fermi surfaces and the nodes of the gap function, respectively.
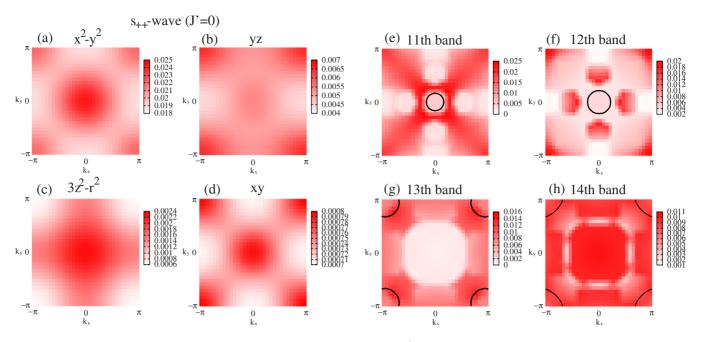
FIG. 7. (Color online) [(a)–(d)] The diagonal components of the gap function $\hat{\Delta}(\mathbf{k})$ in the orbital representation and [(e)–(h)] those in the band representation for $U=0.4$, $U'=1.18$ and $J=0.1$, $J'=0$ eV. The solid and dashed lines represent the Fermi surfaces and the nodes of the gap function, respectively.

to the diagonal components of $\hat{V}(\mathbf{q})<0$ as shown in Fig. 4(c). We call this s-wave state as the s_{++}-wave state. The gap function in the band representation, however, has sign change between the Fermi surfaces and line nodes on the 14th band Fermi surface. These facts reflect that the sign change in the gap function in the orbital representation between the $d_{x^2-y^2}$ diagonal component and the other orbital diagonal components. The 11th band and 12th band Fermi surface has mainly d_{yz} and d_{zx} orbital character while the 13th band Fermi surface has mainly $d_{x^2-y^2}$ orbital character. Therefore, the gap function has different sign between the hole pockets and the 13th band electron pocket. The 14th band electron pocket has mainly d_{yz} and d_{zx} orbital character away from the Brillouin-zone boundary while $d_{x^2-y^2}$ orbital character on the 14th band electron pocket is comparable with d_{yz} and d_{zx} one near the Brillouin-zone boundary. Thus, the gap function on the 14th band electron pockets has plus sign near the zone boundary and minus sign away from the zone boundary. By the simple mean-field analysis of the pair transfer term of the interacting part of the Hamiltonian (3)

$$\frac{J'}{2}\sum_{i,\ell\neq\bar{\ell},\sigma\neq\bar{\sigma}}\langle d^{\dagger}_{i\ell\sigma}d^{\dagger}_{i\ell\bar{\sigma}}\rangle\langle d_{i\bar{\ell}\bar{\sigma}}d_{i\bar{\ell}\sigma}\rangle \propto \sum_{\mathbf{k},\ell\neq\bar{\ell}}\Delta^{AA}_{\ell\ell}(\mathbf{k})\Delta^{AA}_{\bar{\ell}\bar{\ell}}(\mathbf{k}).$$

It is shown that the pair transfer $J'>0$ favors the sign change between the diagonal components of the gap function in the orbital representation.

In fact, we also examine the case with $J'=0$ and we find that the s_{++}-wave state without sing change between the orbitals is realized for $U<U'$. We show the gap function for $U=0.4$, $U'=1.18$, $J=0.1$, and $J'=0$ in Fig. 7. It is found that the all diagonal components of the gap function in the orbital representation have the same sign and those in the band rep-

resentation have no sign change between all Fermi surfaces. Therefore, it is considered that the sign change in the gap function between the $d_{x^2-y^2}$ diagonal component and the others is due to the pair transfer J'.[52,53]

It is helpful for understanding the difference between the $s_{\pm}$-wave state and the s_{++}-wave state in more detail to consider the gap function in the real space. For $s_{\pm}$-wave state, the on-site pairing is comparable with the nearest-neighbor and/or the next-nearest-neighbor one. On the other hand, for the s_{++}-wave state, the on-site pairing is dominant and the off-site pairings are negligibly small as compared to the on-site pairing.

Here we discuss the reason why the on-site part of the gap function for $s_{\pm}$-wave state is large (especially in the $d_{x^2-y^2}$ diagonal component) even though the most dominant component of the effective interaction is always repulsive in $\mathbf{q}$ space [see Fig. 3(c)] and then the on-site effective interaction is repulsive. When we perform the Fourier transformation of the gap equation, Eq. (8), the on-site part of the left-hand side is proportional to the on-site gap function while that of the right-hand side is given by the product of the on-site effective interaction [$\times(-1)$] and the on-site anomalous Green's function which is proportional to the $\mathbf{q}$ summation of the gap-function times the single-particle spectral weight times the thermal factor. In the case with the $d_{x^2-y^2}$ diagonal component, the on-site gap function is negative as the negative contribution of the gap function in $\mathbf{q}$ space is much larger than the positive one as shown in Fig. 5(a). On the other hand, the on-site anomalous Green's function becomes positive as the single-particle spectral weight of the $d_{x^2-y^2}$ hole band is very large around the Γ point where the gap function is positive as compared to that of the electron band around the M point where the gap function is negative. Then, the gap equation can be satisfied with the large value of the
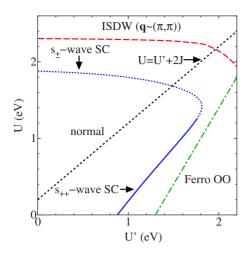
FIG. 8. (Color online) The phase diagram on U'-U plane for $J=J'=0.1$ eV at $x=0.1$ and $T=0.02$ eV. The solid and dotted lines show the s_{++} wave and the $s_{\pm}$-wave superconducting instabilities, respectively. The dashed and dot-dashed lines show instabilities towards the incommensurate spin-density wave and the ferro-orbital order, respectively.

on-site gap function against the repulsive on-site effective interaction.

When the doping x increases, the Fermi level rises apart from the $d_{x^2-y^2}$ hole band and then the effect of the hole band decreases resulting in the decrease in the on-site gap function as well as the decrease in the superconducting transition temperature (not shown). Such doping dependence of the on-site gap function has recently been observed in the five-band Hubbard model.[54] On the contrary, in the s_{++}-wave state, the on-site pairing is always dominant almost independent of the doping x.

E. Phase diagram

The phase diagram on U'-U plane for $J=J'=0.1$ is shown in Fig. 8, where the magnetic and charge-orbital instability is determined by $\det[\hat{1}-\hat{\chi}^{(0)}(\mathbf{q})\hat{S}]=0$ and $\det[\hat{1}-\hat{\chi}^{(0)}(\mathbf{q})\hat{C}]=0$, respectively and the superconducting instability is determined by $\lambda=1$ as mentioned before. The ISDW with $\mathbf{q}\sim(\pi,\pi)$ appears in the large U region while the ferro-orbital order appears for $U<U'$ (Ref. 55) [see also Figs. 3(a), 3(b), 4(a), and 4(b)]. It is noted that on the phase boundary where the charge-orbital instability takes place, the longitudinal orbital susceptibility $[\hat{\chi}^c(\mathbf{q})]^{\alpha\beta}_{\ell\ell,\ell'\ell'}$ diverges while the charge susceptibility $\sum_{\ell,\ell',\alpha,\beta}[\hat{\chi}^c(\mathbf{q})]^{\alpha\beta}_{\ell\ell,\ell'\ell'}$ dose not. The $s_{\pm}$-wave pairing is realized near the ISDW due to the spin fluctuations while the s_{++}-wave pairing is realized near the ferro-orbital ordered phase due to the charge-orbital fluctuations, where we regard the superconducting states as the s_{++}-wave states if d_{yz}, d_{zx}, and $d_{x^2-y^2}$ diagonal components of the gap function have no sign change in $\mathbf{k}$ space and as the $s_{\pm}$-wave states if not. The way to determine whether the superconducting state is the $s_{\pm}$-wave state or the s_{++}-wave state is not unique. This is because the $s_{\pm}$ wave and the s_{++}-wave state are same symmetry (A_{1g}) and the change between s_{++} wave and the $s_{\pm}$-wave state is crossover. In fact,

as U increases, the on-site paring decreases while the off-site pairing increases continuously. At $U\sim1.25$, the nodes appear around the M point for the $d_{x^2-y^2}$ diagonal component and those approaches the Γ point as U increases. It is noted that we also obtain the phase diagram on U'-U plane for $J=J'=0.25$ and find that the phase diagram is essentially the same as that for $J=J'=0.1$ except that the magnetic and the $s_{\pm}$-wave superconducting instabilities are slightly enhanced by the larger value of the Hund's coupling J.

F. Effects of electron-phonon coupling

In this section, we discuss the effects of the electron-phonon coupling. By performing the group theoretical analysis for LaFeAsO, it is found that there are 14 kinds of the optical phonon modes at the Γ point: $2A_{1g}+2B_{1g}+4E_g+3A_{2u}+3E_u$. Here, we concentrate on the A_{1g} mode in which La and As ions oscillate along the c axis. The A_{1g} phonon dose not break the symmetry of the orbital and the resulting electron-phonon coupling matrix $\hat{g}$ is diagonal in the orbital representation. Within the RPA, the charge-orbital susceptibility $\hat{\chi}^c(\mathbf{q})$ including the effects of both the electron-electron and the electron-phonon couplings is obtained by replacing U with $U-2U_{ph}$ and $2U'-J$ with $2(U'-U_{ph})-J$ in Eqs. (5) and (7), where $U_{ph}=2g^2/\omega_{A_{1g}}$, $\omega_{A_{1g}}$ is the frequency of the A_{1g} phonon and we neglect the orbital and $\mathbf{q}$ dependence of the electron-phonon interaction. It is found that the interorbital direct term U' which enhances the orbital fluctuations is harder to be reduced by the electron-phonon coupling than the intraorbital direct term U. As a result, the orbital fluctuations are relatively enhanced by the electron-phonon coupling as compared to the spin fluctuations.

IV. SUMMARY AND DISCUSSION

In summary, we have investigated the pairing symmetry of the two-dimensional 16-band d-p model by using the RPA and have obtained the phase diagram including the magnetic and orbital orders and the superconductivity. For $U>U'$, the $s_{\pm}$-wave superconductivity is realized near the ISDW with $\mathbf{q}\sim(\pi,\pi)$ phase. On the other hand, for $U<U'$, the s_{++}-wave superconductivity appears near the ferro-orbital ordered phase. The $s_{\pm}$-wave pairing is mediated by the spin fluctuations while that the s_{++}-wave pairing is mediated by the orbital fluctuations.

For $U>U'$, the gap function for the $s_{\pm}$-wave pairing changes its sign between the hole pockets and the electron pockets and the most dominant contribution of the gap function is the $d_{x^2-y^2}$ orbital diagonal component. This is qualitatively consistent with the results based on the five-band Hubbard model.[25–30] However, the $d_{x^2-y^2}$ diagonal component of the gap function in our 16-band d-p model have much larger value than the other matrix elements in comparison with the results based on the five-band Hubbard model.[26,28] This may be because the outer hole Fermi surface which has mainly d_{yz} and d_{zx} orbital character obtained by the d-p model is almost circular but that obtained by the five-band Hubbard model is diamond shape.[25] Therefore, the nesting effect which en-

hances the spin fluctuations becomes weak in our d-p model and the resulting components of $\hat{\Delta}(\mathbf{k})$ related to d_{yz}, d_{zx} orbitals have smaller values.

For $U < U'$, the gap function in the orbital representation for the s_{++}-wave pairing dose not change its sign in $\mathbf{k}$ space. In other words, the on-site pairing is much larger than the off-site pairing in the real space. This is similar to the conventional phonon-mediated superconductivity. However, the gap functions have different signs between orbitals in contrast to the conventional phonon-mediated superconductivity. We have shown that this sign change in the gap functions between orbitals is due to the effect of the pair transfer interaction J'.[52,53] It is noted that the s_{++}-wave state has been observed also in the one-dimensional two-band Hubbard model in the same parameter region with $U < U'$.[36]

It seems that the both $s_\pm$ wave and the s_{++}-wave states with full superconducting gaps are consistent with various experiments such as, the NMR relaxation rate, the Knight shift, the ARPES, and the magnetic penetration depth measurements, although the sign of the gap function has not been directly observed there. However, according to the recent theoretical studies of the nonmagnetic impurity effects,[56] Anderson's theorem is violated for the $s_\pm$-wave superconductivity in contrast to the experimental results of very weak T_c suppression in Fe site substitution[10] and neutron irradiation.[16] Since it can be considered that the impurity potential by the Fe-site substitution is diagonal and local in the orbital basis according to the first-principles calculation,[57] it is expected that the s_{++}-wave state observed in the present study is more robust against the nonmagnetic impurity effects than the $s_\pm$-wave state.

In addition to the Coulomb interaction, we have also discussed the effects of the coupling g between the electron and the A_{1g} phonon within the RPA. It has been found that the s_{++}-wave pairing realized in the unrealistic parameter region with $U < U'$ for $g = 0$ is enhanced due to the effect of g and can be expanded over the realistic parameter region with $U > U'$ for a realistic value of g. In the first-principles calculations for iron-based superconductors in conjunction with the Migdal-Eliashberg theory, the electron-phonon coupling is found to be too small to obtain high T_c observed in experiments.[23] The effect of the Coulomb interaction, however, has not been discussed there. In the present study, the cooperative effect of the Coulomb interaction and the electron-phonon coupling is crucial for the enhancement of the orbital fluctuations which induce the s_{++}-wave superconductivity. Recently, the large isotope effects on the transition temperatures for both the SDW and the superconductivity have been observed.[58] This experimental result implies that not only the Coulomb interaction but also the electron-phonon coupling plays crucial effects on the electronic states for iron-based superconductors.

In early theoretical studies for the copper oxide superconductors, the effect of the Coulomb interaction between the d and p electrons U_{pd} was studied by several authors.[59,60] According to the RPA study based on the d-p model with the single $d_{x^2-y^2}$ orbital, U_{pd} enhances the charge fluctuations with $\mathbf{q} = (0,0)$ and the s-wave superconductivity is realized due to the effect of charge fluctuations.[59] In addition, the $1/N$-expansion approaches (N is the spin-orbital degeneracy) revealed that the strong correlation effect enhances the charge fluctuations together with the s-wave superconductivity.[60] Therefore, it is expected that, in the present d-p model with multi d orbitals, U_{pd} enhances the charge-orbital fluctuations which induce the s_{++}-wave superconductivity. The explicit calculations based on the d-p model including not only the on-site Coulomb interaction but also the intersite Coulomb interaction U_{pd} together with the electron-phonon coupling g are now under way.

[1] Y. Kamihara, H. Hiramatsu, M. Hirano, R. Kawamura, H. Yanagi, T. Kamiya, and H. Hosono, J. Am. Chem. Soc. **128**, 10012 (2006).

[2] Y. Kamihara, T. Watanabe, M. Hirano, and H. Hosono, J. Am. Chem. Soc. **130**, 3296 (2008).

[3] G. F. Chen, Z. Li, D. Wu, G. Li, W. Z. Hu, J. Dong, P. Zheng, J. L. Luo, and N. L. Wang, Phys. Rev. Lett. **100**, 247002 (2008).

[4] Z. A. Ren, J. Yang, W. Lu, W. Yi, G. C. Che, X. L. Dong, L. L. Sun, and Z. X. Zhao, Mater. Res. Innovations **12**, 105 (2008).

[5] Z. A. Ren, J. Yang, W. Lu, W. Yi, X. L. Shen, Z. C. Li, G. C. Che, X. L. Dong, L. L. Sun, F. Zhou, and Z. X. Zhao, EPL **82**, 57002 (2008).

[6] X. H. Chen, T. Wu, G. Wu, R. H. Liu, H. Chen, and D. F. Fang, Nature (London) **453**, 761 (2008).

[7] Z. A. Ren, W. Lu, J. Yang, W. Yi, X. L. Shen, Z. C. Li, G. C. Che, X. L. Dong, L. L. Sun, F. Zhou, and Z. X. Zhao, Chin.

Phys. Lett. **25**, 2215 (2008).

[8] C. de la Cruz, Q. Huang, J. W. Lynn, J. Li, W. Ratcliff II, J. L. Zarestky, H. A. Mook, G. F. Chen, J. L. Luo, N. L. Wang, and P. Dai, Nature (London) **453**, 899 (2008).

[9] K. Matano, Z. A. Ren, X. L. Dong, L. L. Sun, Z. X. Zhao, and G. Q. Zheng, EPL **83**, 57001 (2008).

[10] A. Kawabata, S. C. Lee, T. Moyoshi, Y. Kobayashi, and M. Sato, J. Phys. Soc. Jpn. **77**, 103704 (2008).

[11] K. Hashimoto, T. Shibauchi, T. Kato, K. Ikada, R. Okazaki, H. Shishido, M. Ishikado, H. Kito, A. Iyo, H. Eisaki, S. Shamoto, and Y. Matsuda, Phys. Rev. Lett. **102**, 017002 (2009).

[12] G. Mu, X. Zhu, L. Fang, L. Shan, C. Ren, and H. H. Wen, Chin. Phys. Lett. **25**, 2221 (2008).

[13] H. Liu, W. Zhang, L. Zhao, X. Jia, J. Meng, G. Liu, X. Dong, G. F. Chen, J. L. Luo, N. L. Wang, W. Lu, G. Wang, Y. Zhou, Y. Zhu, X. Wang, Z. Xu, C. Chen, and X. J. Zhou, Phys. Rev. B **78**,

184514 (2008).

[14] H. Ding, P. Richard, K. Nakayama, T. Sugawara, T. Arakane, Y. Sekiba, A. Takayama, S. Souma, T. Sato, T. Takahashi, Z. Wang, X. Dai, Z. Fang, G. F. Chen, J. L. Luo, and N. L. Wang, EPL **83**, 47001 (2008).

[15] T. Kondo, A. F. Santander-Syro, O. Copie, C. Liu, M. E. Tillman, E. D. Mun, J. Schmalian, S. L. Bud'ko, M. A. Tanatar, P. C. Canfield, and A. Kaminski, Phys. Rev. Lett. **101**, 147003 (2008).

[16] A. Karkin, J. Werner, G. Behr, and B. Goshchitskii, arXiv:0904.1634 (unpublished).

[17] Y. Nakai, K. Ishida, Y. Kamihara, M. Hirano, and H. Hosono, J. Phys. Soc. Jpn. **77**, 073701 (2008).

[18] Y. Kobayashi, A. Kawabata, S. C. Lee, T. Moyoshi, and M. Sato, J. Phys. Soc. Jpn. **78**, 073704 (2009).

[19] S. Lebegue, Phys. Rev. B **75**, 035110 (2007).

[20] D. J. Singh and M. H. Du, Phys. Rev. Lett. **100**, 237003 (2008).

[21] K. Haule, J. H. Shim, and G. Kotliar, Phys. Rev. Lett. **100**, 226402 (2008).

[22] G. Xu, W. Ming, Y. Yao, X. Dai, S.-C. Zhang, and Z. Fang, EPL **82**, 67002 (2008).

[23] L. Boeri, O. V. Dolgov, and A. A. Golubov, Phys. Rev. Lett. **101**, 026403 (2008).

[24] I. I. Mazin, D. J. Singh, M. D. Johannes, and M. H. Du, Phys. Rev. Lett. **101**, 057003 (2008).

[25] K. Kuroki, S. Onari, R. Arita, H. Usui, Y. Tanaka, H. Kontani, and H. Aoki, Phys. Rev. Lett. **101**, 087004 (2008).

[26] K. Kuroki, S. Onari, R. Arita, H. Usui, Y. Tanaka, H. Kontani, and H. Aoki, New J. Phys. **11**, 025017 (2009).

[27] K. Kuroki, H. Usui, S. Onari, R. Arita, and H. Aoki, Phys. Rev. B **79**, 224511 (2009).

[28] T. Nomura, J. Phys. Soc. Jpn. **78**, 0347160 (2009).

[29] H. Ikeda, J. Phys. Soc. Jpn. **77**, 123707 (2008).

[30] F. Wang, H. Zhai, Y. Ran, A. Vishwanath, and D. H. Lee, Phys. Rev. Lett. **102**, 047005 (2009).

[31] S. Graser, T. A. Maier, P. J. Hirschfeld, and D. J. Scalapino, New J. Phys. **11**, 025016 (2009).

[32] Z. J. Yao, J. X. Li, and Z. D. Wang, New J. Phys. **11**, 025009 (2009).

[33] T. D. Stanescu, V. Galitski, and S. Das Sarma, Phys. Rev. B **78**, 195114 (2008).

[34] V. Cvetkovic and Z. Tesanovic, EPL **85**, 37002 (2009).

[35] K. Seo, B. A. Bernevig, and J. Hu, Phys. Rev. Lett. **101**, 206404 (2008).

[36] K. Sano and Y. Ōno, J. Phys. Soc. Jpn. **78**, 124706 (2009).

[37] V. Vildosola, L. Pourovskii, R. Arita, S. Biermann, and A. Georges, Phys. Rev. B **78**, 064518 (2008).

[38] K. Nakamura, R. Arita, and M. Imada, J. Phys. Soc. Jpn. **77**, 093711 (2008).

[39] Y. Yanagi, Y. Yamakawa, and Y. Ōno, J. Phys. Soc. Jpn. **77**,

123701 (2008).

[40] Y. Yanagi, Y. Yamakawa, and Y. Ōno, Proceedings of Ninth International Conference on Materials and Mechanisms of Superconductivity, Tokyo, 2009 (unpublished).

[41] J. P. Perdew, K. Burke, and M. Ernzerhof, Phys. Rev. Lett. **77**, 3865 (1996).

[42] P. Blaha, K. Schwarz, G. Madsen, D. Kvasnicka, and J. Luitz, *wien2k, An Argumented Plane Wave Plus Local Orbitals Program for Calculating Crystal Properties* (Technische Universiat, Wien, Austria, 2002), http://www.wien2k.at

[43] T. Nomura, S. W. Kim, Y. Kamihara, M. Hirano, P. V. Sushko, K. Kato, M. Takata, A. L. Shluger, and H. Hosono, Supercond. Sci. Technol. **21**, 125028 (2008).

[44] Y. Yamakawa, Y. Yanagi, and Y. Ōno (unpublished).

[45] C. Cao, P. J. Hirschfeld, and H. P. Cheng, Phys. Rev. B **77**, 220506(R) (2008).

[46] E. Manousakis, J. Ren, S. Meng, and E. Kaxiras, Phys. Rev. B **78**, 205112 (2008).

[47] H. Tang, M. Plihal, and D. L. Millsh, J. Magn. Magn. Mater. **187**, 23 (1998).

[48] T. Takimoto, T. Hotta, and K. Ueda, Phys. Rev. B **69**, 104504 (2004).

[49] M. Mochizuki, Y. Yanase, and M. Ogata, Phys. Rev. Lett. **94**, 147005 (2005).

[50] K. Yada and H. Kontani, J. Phys. Soc. Jpn. **74**, 2161 (2005).

[51] The spin and charge-orbital susceptibilities are the particle-hole channel while the superconducting susceptibility is the particle-particle channel. Then, there is a rotation of the orbital indices of the effective pairing interaction V in the gap equation, Eq. (8) with respect to those of the spin and charge-orbital susceptibilities in Eqs. (4)–(6). This is more explicitly represented in Ref. 31 with a different notation.

[52] J. Kondo, Prog. Theor. Phys. **29**, 1 (1963).

[53] K. Yamaji and S. Abe, J. Phys. Soc. Jpn. **56**, 4237 (1987).

[54] T. Kariyado and M. Ogata, arXiv:0911.2959 (unpublished).

[55] The pattern of the orbital order should be determined by a self-consistent method such as the Hartree-Fock calculation. Our detailed study of the orbital order by using the Hartree-Fock approximation is underway. N. Adachi, Y. Yamakawa, Y. Yanagi, and Y. Ōno (unpublished).

[56] S. Onari and H. Kontani, Phys. Rev. Lett. **103**, 177001 (2009).

[57] A. F. Kemper, C. Cao, P. J. Hirschfeld, and H.-P. Cheng, Phys. Rev. B **80**, 104511 (2009).

[58] R. H. Liu, T. Wu, G. Wu, H. Chen, X. F. Wang, Y. L. Xie, J. J. Yin, Y. J. Yan, Q. J. Li, B. C. Shi, W. S. Chu, Z. Y. Wu, and X. H. Chen, Nature (London) **459**, 64 (2009).

[59] P. B. Littlewood, C. M. Varma, and E. Abrahams, Phys. Rev. Lett. **63**, 2602 (1989).

[60] D. S. Hirashima, Y. Ōno, T. Matsuura, and Y. Kuroda, J. Phys. Soc. Jpn. **61**, 649 (1992).